γ-Mn at the border between weak and strong correlations

I. Di Marco,[1,2,*] J. Minár,[3] J. Braun,[3] M. I. Katsnelson,[1] A. Grechnev,[4] H. Ebert,[3] A. I. Lichtenstein,[5] and O. Eriksson[2]

[1] *Institute for Molecules and Materials, Radboud University of Nijmegen, NL-6525 ED Nijmegen, The Netherlands*
[2] *Department of Physics and Materials Science, Uppsala University, Box 530, SE-751 21 Uppsala, Sweden*
[3] *Department Chemie und Biochemie, Physikalische Chemie, Ludwig-Maximilians Universität München, D-81377 München, Germany*
[4] *B. Verkin Institute for Low Temperature Physics and Engineering, 47 Lenin Avenue, Kharkov, Ukraine*
[5] *Institute of Theoretical Physics, University of Hamburg, 20355 Hamburg, Germany*

(Dated: June 11, 2013)

We investigate the role of magnetic fluctuations in the spectral properties of paramagnetic γ-Mn. Two methods are employed. The Local Density Approximation plus Dynamical Mean-Field Theory together with the numerically exact quantum Monte-Carlo solver is used as a reference for the spectral properties. Then the same scheme is used with the computationally less demanding perturbative spin-polarized fluctuation-exchange solver in combination with the Disordered Local Moment approach, and photoemission spectra are calculated within the one-step model. It is shown that the formation of local magnetic moments in γ-Mn is very sensitive to the value of Hund's exchange parameter. Comparison with the experimental photoemission spectra demonstrates that γ-Mn is a strongly correlated system, with the Hubbard band formation, which cannot be described by the perturbative approach. However, minor change of parameters would transform it into a weakly correlated system.

PACS numbers: 71.20.Be, 75.10.Lp, 79.60.-i

arXiv:0906.0787v1 [cond-mat.str-el] 3 Jun 2009

I. INTRODUCTION

Itinerant electron magnetism has been a long-standing problem in solid state physics, due to the coexistence of itinerant and localized features in the behavior of magnetic d-electrons[1,2,3]. The standard *ab initio* approach to many-electron systems, i.e. the Density-Functional Theory (DFT) in Local Density Approximation (LDA), or Generalized Gradient Approximation (GGA)[4], describes the ground state properties of magnetic $3d$ metals reasonably well, but has serious problems with the description of excitation spectra, e.g., photoemission spectra of nickel, and also with the electronic structure and magnetism of iron, cobalt, and nickel at finite temperatures[5]. Correlation effects are essential also in other $3d$ itinerant-electron magnets, such as half-metallic ferromagnets[6].

A qualitative theory of itinerant-electron magnets taking into account the duality of localized and itinerant behavior was developed in a framework of the Hubbard model[3]. While this theory gave us a deep insight, it is insufficient to describe qualitatively properties of specific magnetic materials taking into account peculiarities of their real electronic structure.

In the last decade much progress has been made with the introduction of the Dynamical-Mean Field Theory (DMFT)[7,8], which allows for a quantitative solution of a lattice many-body problem with the inclusion of all local quantum dynamical fluctuations. The LDA+DMFT scheme, arising from the combination of the DMFT and standard DFT-LDA, has been successfully applied to describe the electronic structure and magnetic properties of Fe and Ni[5,9,10]. In particular an excellent quantitative description of Ni was obtained (see also Refs. 11,12), while for Fe the situation is slightly worse. This is not surprising, since in Fe the role of non-local effects (beyond DMFT) is more important than in Ni, as follows from direct photoemission data on the effective mass renormalization in different points of the Brillouin zone[13].

Besides Fe and Ni, the electronic structure and magnetic properties of γ-Mn are especially interesting. This phase appears between $T = 1368\,\mathrm{K}$ and $T = 1406\,\mathrm{K}$, but can be stabilized down to room temperature through the addition of a small amount of impurities[14] or as layer-by-layer deposition on $Cu_3Au(100)$[15,16]. Below the Neél temperature, about 540 K, γ-Mn becomes antiferromagnetic, which is accompanied by a tetragonal distortion into the fct structure[15,17]. Among all transition metals, γ-Mn shows the largest discrepancy between the computational DFT-LDA (or GGA) predictions for the lattice constant and bulk modulus, and the experimental data[18,19,20]. Tetragonal distortion and anomalies in the bulk modulus are good indications of strong electron correlations, and Zein[21] has pointed out that the correlation effects in the $3d$-shell are stronger at half-filling. In fact we have recently proved that inclusion of proper many-body effects through LDA+DMFT leads to correct equilibrium volume and bulk modulus[12]. Moreover, Biermann *et al.*[16] have successfully applied the LDA+DMFT scheme to the angle-resolved photoemission spectra (ARPES) of γ-Mn, emphasizing the formation of a three-peak structure characteristic for strongly correlated systems. These calculations were carried out with the numerically exact quantum Monte-Carlo (QMC) solver, but, unfortunately, this technique is computationally quite expensive, especially, if one is interested in the regime of relatively low temperatures, such as

room temperature. In addition, it uses a truncated multi-band Hubbard Hamiltonian, and involves many technical problems, e.g., with analytical continuation (for a more detailed discussion, see Ref. 22).

In the present paper we address the question to which extent such a regime of strong correlations can be studied by means of a simpler implementation. In particular, the spin-polarized T-matrix fluctuation-exchange solver (SPTF)[23,24] was implemented to treat the problem of magnetic fluctuations in transition metals, and has been successfully applied to the ferromagnetic phases of Fe, Co, Ni[11,24,25] and the anti-ferromagnetic phase of γ-Mn[12], as well as to half-metallic ferromagnets[6]. It is quite stable, computationally cheap and deals with the complete four-indices interaction matrix. On the other hand, its perturbative character restricts its use to relatively weakly, or moderately, correlated systems.

Not surprisingly, the SPTF performs well when starting from a spin-polarized solution, since the spin-splitting contains already the main part of the exchange and correlation effects. Conversely, the direct application of SPTF to a non-magnetic phase can create stability problems since we are trying, in this case, to attribute strong, and essentially mean-field, effect of formation of local magnetic moment to dynamical fluctuations around non-spin-polarized state. This is appropriate when one uses the QMC method, which has no formal restrictions on the amplitude of fluctuations, but seems problematic for the perturbative approaches.

As a way to weaken such a limitation we propose a combination of SPTF with the disordered local moment (DLM) approach[26,27]. As already shown for the case of actinides[28] the inclusion of the fluctuations of randomly oriented local moments can improve drastically the description of energetics in the paramagnetic phase. One can hope therefore that it allows us to extend the range of applicability of SPTF.

As we show here, the results appear to be strongly dependent on the formation of local moments, which is driven by the Hund's exchange. For realistic values of the Coulomb interaction γ-Mn is shown to be a material right at the border between weak and strong correlations.

II. METHOD

In the LDA+DMFT scheme we correct the one-particle LDA Hamiltonian with an additional two-particle term, which explicitly describes the local Coulomb repulsions between a given set of correlated orbitals. The latter are usually associated to electrons in narrow bands, not properly described in the LDA. Naming $\mathbf{R}$ the lattice sites, the Hamiltonian becomes

$$\hat{H} = \hat{H}_{\mathrm{LDA}} + \frac{1}{2}\sum_{\mathbf{R}}\sum_{1,2,3,4} U_{1,2,3,4}\hat{c}^{\dagger}_{\mathbf{R},1}\hat{c}^{\dagger}_{\mathbf{R},2}\hat{c}_{\mathbf{R},4}\hat{c}_{\mathbf{R},3}, \quad (1)$$

where the second sum runs over the quantum numbers of the chosen orbitals. The system in eq. (1) represents an "effective" Hubbard model, whose solution is a complicated many-body problem. The main observable is the local Green's function $G(i\omega_n)$, which can be obtained from the self-energy $\Sigma(i\omega_n)$ by means of the Dyson equation. Here and below $i\omega_n$ are the Matsubara frequencies for finite temperature many-body formalism. In the DMFT the self-energy is obtained by mapping the original lattice problem onto a problem of an atomic site coupled to an electronic bath, i.e. the effective Anderson impurity model. The equality of the local Green's function in the original and the fictitious system assures the self-consistent condition that determines the bath. In the DMFT the self-energy $\Sigma(i\omega_n)$ is purely local in real space, and consequently is $\mathbf{k}$-independent in the momentum space, which becomes exact in the limit of infinite space dimensionality. Finally, notice that the Hamiltonian in eq. (1) is constructed on top of the LDA Hamiltonian, which should already contain all the effects of the Coulomb repulsions in the form of a mean-field. Thus, we remove from the self-energy those contributions already included to avoid counting them twice. For treating metals the most common choice for the so-called "double counting" correction is the static part of the self-energy[11,24], averaged over the orbital indices for each spin channel.

In the present paper we have used two different LDA+DMFT implementations. The first one is the LDA+DMFT code of Refs. 12,25, based on the full-potential linear muffin-tin orbital (FP-LMTO) method[29]. We have used it for the QMC simulations, after having implemented the Hirsch-Fye Quantum Monte-Carlo algorithm of Refs. 5,30. The second code is based of the full-potential Korringa-Kohn-Rostoker (FP-KKR) multiple-scattering theory, and has been used for the DLM+SPTF simulations[31]. The LDA+DMFT simulations with the SPTF solver were made using both these codes, and the results are practically identical, consistently with our recent findings for the ground-state properties of Ni and Mn[12].

The reason behind this twofold approach lays in the simplicity of the corresponding implementations. In QMC the interval $[0,\beta]$ on the axis of the imaginary time τ is discretized in L time-slices. The fully interacting Green's function is evaluated only for the chosen τ, and then transformed to Matsubara frequencies. Due to the statistical error, typical of Monte-Carlo methods, and to the Trotter error, associated to the imaginary time-discretization, the resulting $G(i\omega_n)$ has bad analytical properties. While for FP-LMTO this is a minor issue, in FP-KKR it is a serious problem, since the LDA+DMFT cycle involves analytical continuation from Matsubara axis to a semi-circular contour[31].

For DLM+SPTF the situation is inverted. In DLM the itinerant electrons form self-maintaining "local moments" which are analogous - but physically different - to the localized spins of the Heisenberg model. Being $\hat{\mathbf{e}}_i$ the orientations of the moments at the sites i, we can describe the system through the generalized grand-

canonical potential $\Omega(\{\hat{\mathbf{e}}_i\})$. Then a mean-field approximation of the true potential is constructed as expansion around a single-site spin Hamiltonian[32]:

$$\Omega_0(\{\hat{\mathbf{e}}_i\}) = -\sum_i \mathbf{h}_i \hat{\mathbf{e}}_i. \quad (2)$$

The self-consistent parameters h_i define a set of probabilities $P_i(\hat{\mathbf{e}}_i)$ of finding the moments oriented towards $\hat{\mathbf{e}}_i$. Explicit calculations can now be made through standard methods used for substitutionally disordered alloys, as the Coherent Potential Approximation (CPA), which has straightforward implementation in the multiple-scattering theory of KKR[31]. On the other hand implementations of DLM into LMTO are more cumbersome, and involve the passage to a Green's function formalism[33].

Finally, for a direct comparison between theory and experiment, photoemission spectra are produced within the so-called one-step model[34,35], which has been recently implemented in combination with the LDA+DMFT using the KKR method[11]. The main idea is to describe the excitation process, the movement of the electron towards the surface, and the final escape from the surface, as a single quantum-mechanically coherent process, which is comprehensive of all the multiple scattering events.

To allow comparison with previous LDA+DMFT results and experimental data, we assumed a face centered tetragonal structure with lattice constant $a = 7.143$ a.u. and a tetragonal distortion corresponding to $c/a = 0.93$. We have included $4s$, $4p$ and $3d$ in the valence electrons; all the other states were considered as core states. In the FP-LMTO basis functions with three tail energies κ were used, while in FP-KKR scattering matrix elements up to $l_{max} = 3$ were included. Only negligible differences could be found in comparing the LDA results.

In the LDA+DMFT simulation, the local Hubbard interaction was applied to the $3d$ electrons. In this case the U-matrix of eq. (1) can be parametrized by means of only two parameters U and J, which were varied among a wide range of reasonable values. In fact the determination of U is a quite serious problem, and usually semi-empirical values are assumed[36]. We have studied configurations corresponding to different parameters through QMC at temperature ranging from $T \simeq 2000$ K down to $T \simeq 500$ K. Convergence in the number of time-slices has been checked, and for high U values or low temperature a number of $L = 128$ time slices has been used. The number of Monte-Carlo sweeps has been set to 500000, while its convergency has been checked up to 10^7.

III. RESULTS

In fig. 1 we show the density of states of the $3d$ electrons obtained through maximum-entropy method. In the bottom of the figure we have used an exchange parameter $J = 0.9$ eV, and the results reproduce quite reasonably the three-peak structure of Ref. 16. By turning

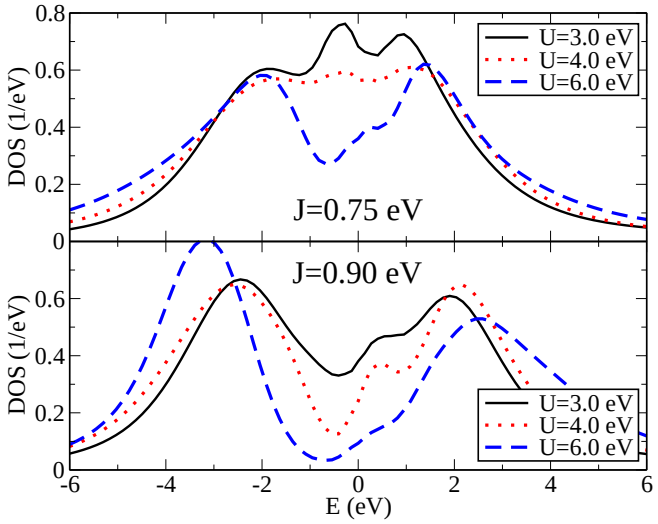

FIG. 1: (colour on-line) Density of states of the $3d$ electrons of γ-Mn from QMC in the LDA+DMFT scheme for $T = 2000$ K. In the top plot results for $J = 0.75$ eV and U changing from 3 eV to 6 eV are shown. In the bottom plot results for $J = 0.9$ eV and same U as above are shown. Notice the big impact of small variations of J on the final spectrum.

on the Coulomb repulsion U, two split Hubbard bands are formed and a quasiparticle resonance appears close to the Fermi level. In comparison to the cited results, our central peak is almost completely smeared out because of the high temperature, but still its foot-print can be seen in the spectrum. In the top of fig. 1 we have presented the density of states for the same simulations, but with a slightly different exchange $J = 0.75$ eV. Strong differences can be observed: the system can form Hubbard bands only for a very strong U and the energy separation between them is smaller than the bare U. While for high J the electrons are observed to redistribute equally among all the orbitals in a way to minimize the QMC double occupation, for small J this does not happen and the occupations of the $3d$ orbitals stay closer to the original LDA picture. This behavior is related with the formation of local magnetic moments, as it will be discussed below. Note that the transition from $J = 0.9$ eV to $J = 0.75$ eV looks small but, actually, it is very essential since it increases the difference $U - 3J$ by a factor of 2.5 which is the energy of the Coulomb interaction between electrons with parallel spins in different orbital states[22].

The problem is that the transition between these two regimes happens close to the real physical value of J. For all the $3d$ transition metals the semi-empirical atomic value $J = 0.9$ eV is commonly used[36], but some calculations suggest that a lower value can be more adequate[37,38].

More information about the different physical situations can be obtained by looking at the square of the local moment $\langle M_z^2 \rangle$, which in QMC is associated to the local spin correlation function. This moment depends

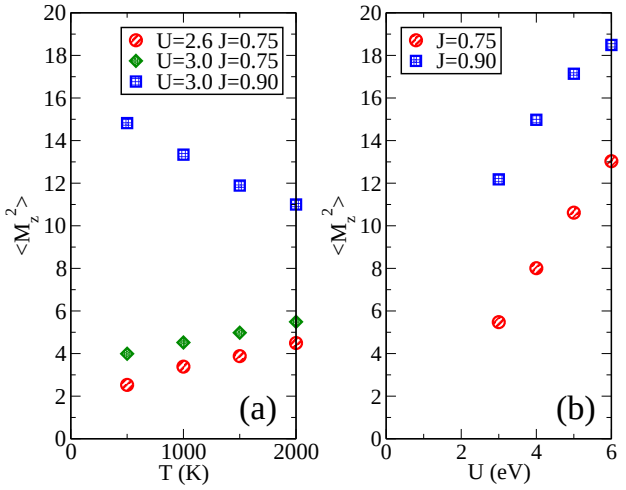

FIG. 2: (colour on-line) (a) Variation of the squared local moment $\langle M_z^2 \rangle$ as a function of T for chosen values of U and J. (b) Variation of the squared local moment $\langle M_z^2 \rangle$ as a function of U at $T = 2000\,\mathrm{K}$.

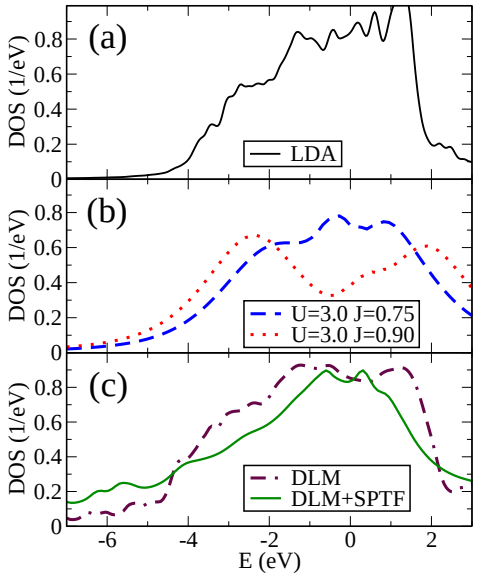

FIG. 3: (colour on-line) Comparison of the significant density of states of the $3d$ electrons presented in the paper: (a) DFT-LDA (b) QMC with $U = 3.0\,\mathrm{eV}$ and different values of J. (c) DLM and DLM+SPTF for $U = 3.0\,\mathrm{eV}$ and $J = 0.8\,\mathrm{eV}$.

strongly on the temperature, as we can see in fig. 2(a) for three pairs of parameters U and J. For very high temperatures T, i.e. for T bigger than U, we expect the system to show a contribution to the effective Curie constant of about 0.5 for each orbital, which corresponds to local spins decoupled from each other[39]. In fact this is the tendency we observe in our calculations, not shown in the figure. For low temperature, i.e. in the interval between 2000 K and 500 K, the physics of manganese is strongly dependent on J. For low J the spin fluctuations are decreased because of the presence of strong orbital fluctuations[40], which become important when the temperature becomes lower. The electrons tend to behave as a Pauli paramagnet, and the local moment decreases together with the temperature. Conversely for high J the electrons tend to localize in each band independently, resulting in the suppression of the orbital fluctuations. As a result a strong fluctuating local moment can form. These different tendencies have been well studied in the two-orbital Hubbard model[40], and it is interesting to see how they can be found in a real material with five (almost) degenerate orbitals and realistic hybridization. Notice that the experimental local magnetic moment is equal to 2.3 Bohr magnetons. In fig. 2(b) we can see the trend of the local moments for different values of U in the two different regimes.

In fig. 3 a comparison of all the significant density of states of our work is presented. The upper panel (a) and the middle panel (b) display respectively the bare LDA results and the LDA+DMFT results with the QMC solver for $U = 3\,\mathrm{eV}$ and $J = 0.75\,\mathrm{eV}$ or $J = 0.9\,\mathrm{eV}$. In the lower panel (c) the density of states obtained within the DLM approach is reported, both for LDA and LDA+DMFT with the SPTF solver ("DLM+SPTF"). While bare DLM describes the fluctuations in a very simple way, still a sort of three peak structure is observed. However the width of the $3d$ band is too big, since it descends from the single particle LDA density of states. In DLM+SPTF we can properly describe the shrinking of the $3d$ band, as already observed for Fe, Co and Ni[25]. In comparison with the QMC calculations, the peak at around $-2\,\mathrm{eV}$ is less pronounced. This depends on the perturbative nature of SPTF, which tends to shift the correlation effects related to the formation of non-coherent satellites. For example, the famous $-6\,\mathrm{eV}$ satellite of Ni is positioned at about $-8\,\mathrm{eV}$. For Mn part of the spectral weight is transferred to the region between -4 and $-6\,\mathrm{eV}$. While DLM+SPTF can reproduce very well the density of states for moderately correlated regimes, the appearance of the Hubbard bands observed in the QMC simulation for high J cannot be reproduced in this approach.

On the basis of these considerations, we can look at the photoemission spectra reported in fig. 4, together with the experimental data of Ref. 16. The spectra are considered at normal emission along the (100) direction, and for photon energies ranging from 14 eV and 70 eV, which corresponds to the $\Gamma - X$ path in the Brillouin zone. In the experimental data we can observe a pronounced peak close to the Fermi energy and a non-dispersive "Hubbard band" at around $-2.8\,\mathrm{eV}$, whose intensity increases for high photon energies. The DLM simulation can describe these features only partially. First the "quasiparticle peak" close to the Fermi energy seems to be much broader than its experimental counterpart. In second place a weak Hubbard band appears at around $-4.5\,\mathrm{eV}$, which is an energy significantly higher than $-2.8\,\mathrm{eV}$. In addition at high photon energies the signal is mixed with a stronger contribution coming from the *sp* band, which

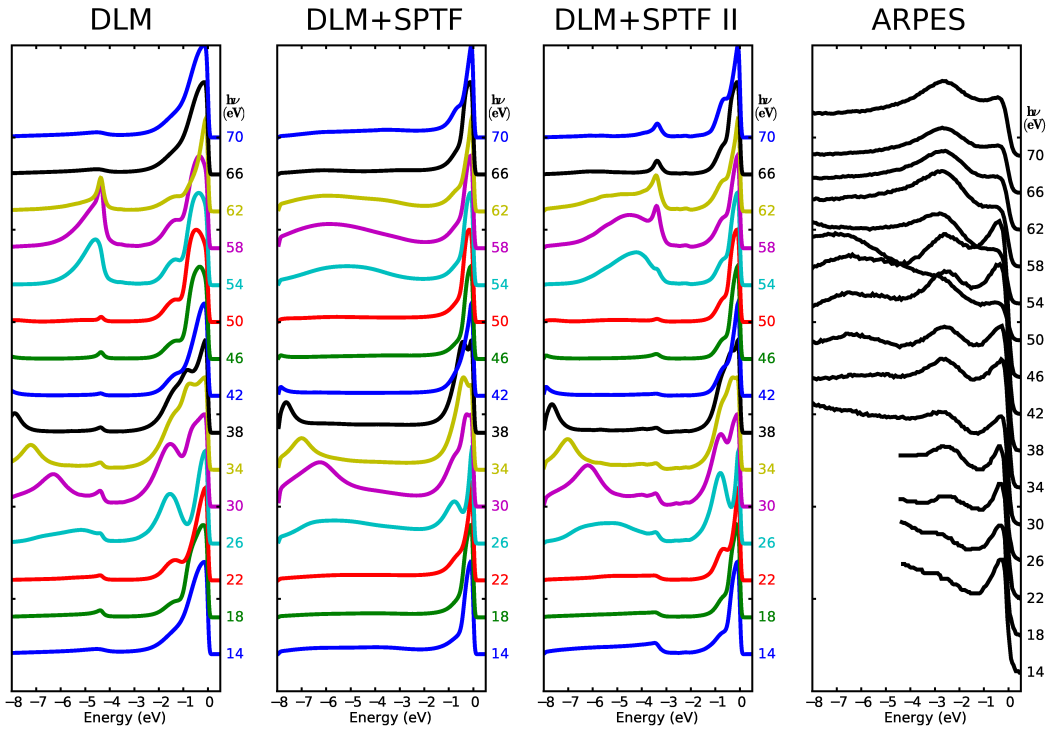

FIG. 4: (colour on-line) Photoemission spectrum along the (100) direction in normal emission for photon energies between 14 eV and 70 eV, which corresponds to the $\Gamma - X$ path in the Brillouin zone. The experimental data of Ref. 16 are compared with calculations within the one-step model based on DLM and DLM+SPTF. In the spectra of the column labelled DLM+SPTF II the imaginary part of the self-energy coming from DMFT has been removed.

makes it difficult to identify this feature with an effective Hubbard band. The use of the DLM+SPTF approach improves essentially the description of the states near the Fermi energy but smears completely the Hubbard band. Probably, this is due to an overestimation of the imaginary part of self-energy for larger excitation energies. Indeed, if one takes into account only the real part of the self energy (DLM+SPTF II) the description of the photoemission spectra can be drastically improved. This reminds of a situation with the GW calculations where neglecting the electron state damping sometimes essentially improves the results[41]. Now we clearly observe a non-dispersive feature at -3.5 eV, which is separated from *sp* contributions, and can be surely identified as an effect of strong correlations. Nevertheless the peak appears at higher binding energy than in the experiment, due to the perturbative nature of SPTF. Finally notice that our simulations emphasize that the peak at the Fermi level possesses a strong surface contribution, visible in all the spectra as a small shoulder, and particularly sensitive to the modeling of the surface barrier of the photoemission process.

In conclusion real manganese is a strongly correlated metal, with Hubbard bands[16]. In such cases, instead of the cumbersome and computationally expensive QMC calculations, the DLM+SPTF approach can be used to describe adequately the energy spectrum close enough to the Fermi energy, but not in the whole energy range. For moderately correlated systems, which were modelled here by variation of J, the DLM+SPTF approach turns out to be adequate for the whole spectrum.

Acknowledgments

We are grateful to B. Gyorffy, J. Staunton, S. Biermann and L. Pourovskii for all their suggestions and interest. Further we are thankful to A. I. Poteryaev for the usage of the QMC code, and to O. Rader for the access to the experimental data of Ref. 16. This work was sponsored by the Stichting Nationale Computerfaciliteiten (National Computing Facilities Foundation, NCF) for the use of the supercomputer facilities, with financial support from the Nederlandse Organisatie voor Wetenschappelijk Onderzoek (Netherlands Organization for Scientific Research, NWO). The programming work was carried out under the HPC-EUROPA++ project (application number 1122), with the support of European Community - Research Infrastructure Action of the FP7. Fundamental support was also given by the Deutsche Forschungsgemeinschaft within the priority program "Moderne und universelle first-principles-Methoden für Mehrelektronensysteme in Chemie und

Physik" (SPP 1145/2).

---

* Electronic address: igor.dimarco@fysik.uu.se

[1] C. Herring, *Exchange interactions among itinerant electrons* (Academic Press, New York, 1966), vol. 4 of *Magnetism*.

[2] S. V. Vonsovsky, *Magnetism*, vol. 2 (Wiley, New York, 1974).

[3] T. Moriya, *Spin Fluctuations in Itinerant Electron Magnetism*, no. 56 in Springer Series in Solid-State Science (Springer-Verlag, Berlin, Heidelberg, New York and Tokyo, 1985).

[4] R. M. Martin, *Electronic Structure: Basic Theory and Practical Methods* (Cambridge University Press, Cambridge, 2004).

[5] A. I. Lichtenstein, M. I. Katsnelson, and G. Kotliar, Phys. Rev. Lett. **87**, 067205 (2001).

[6] M. I. Katsnelson, V. Y. Irkhin, L. Chioncel, A. I. Lichtenstein, and R. A. de Groot, Rev. Mod. Phys. **80**, 315 (2008).

[7] A. Georges, G. Kotliar, W. Krauth, and M. J. Rozenberg, Rev. Mod. Phys. **68**, 13 (1996).

[8] G. Kotliar, S. Savrasov, K. Haule, V. Oudovenko, O. Parcollet, and C. Marianetti, Rev. Mod. Phys. **78**, 865 (2006).

[9] M. I. Katsnelson and A. I. Lichtenstein, J. Phys.: Condens. Matter **11**, 1037 (1999).

[10] M. I. Katsnelson and A. I. Lichtenstein, Phys. Rev. B **61**, 8906 (2000).

[11] J. Braun, J. Minár, H. Ebert, M. I. Katsnelson, and A. I. Lichtenstein, Phys. Rev. Lett. **97**, 227601 (2006).

[12] I. Di Marco, J. Minár, S. Chadov, M. I. Katsnelson, H. Ebert, and A. I. Lichtenstein, Phys. Rev. B **79**, 115111 (pages 14) (2009).

[13] J. Schäfer, M. Hoinkis, E. Rotenberg, P. Blaha, and R. Claessen, Phys. Rev. B **72**, 155115 (2005).

[14] Y. Endoh and Y. Ishikawa, J. Phys. Soc. Japan **30**, 1614 (1971).

[15] B. Schirmer, B. Feldmann, A. Sokoll, Y. Gauthier, and M. Wuttig, Phys. Rev. B **60**, 5895 (1999).

[16] S. Biermann, A. Dallmeyer, C. Carbone, W. Eberhardt, C. Pampuch, O. Rader, M. I. Katsnelson, and A. I. Lichtenstein, Pis'ma ZhETF **80**, 714 (2004), [JETP Letters **80**, 614 (2004)].

[17] T. Oguchi and A. J. Freeman, J. Magn. Magn. Mater. **46**, L1 (1984).

[18] V. L. Moruzzi and P. M. Marcus, Phys. Rev. B **48**, 7665 (1993).

[19] M. Eder, J. Hafner, and E. G. Moroni, Phys. Rev. B **61**, 11492 (2000).

[20] J. Hafner and D. Spišák, Phys. Rev. B **72**, 144420 (2005).

[21] N. E. Zein, Phys. Rev. B **52**, 11813 (1995).

[22] K. Held, Adv. Phys. **56**, 829 (2007).

[23] L. V. Pourovskii, M. I. Katsnelson, and A. I. Lichtenstein, Phys. Rev. B **72**, 115106 (2005).

[24] M. I. Katsnelson and A. I. Lichtenstein, Eur. Phys. J. B **30**, 9 (2002).

[25] A. Grechnev, I. Di Marco, M. I. Katsnelson, A. I. Lichtenstein, J. Wills, and O. Eriksson, Phys. Rev. B **76**, 035107 (2007).

[26] B. L. Gyorffy, A. J. Pindor, J. Staunton, G. M. Stocks, and H. Winter, J. Phys. F: Met. Phys. **15**, 1337 (1985).

[27] J. Staunton, B. L. Gyorffy, G. M. Stocks, and J. Wadsworth, J. Phys. F: Met. Phys. **16**, 1761 (1986).

[28] A. M. N. Niklasson, J. M. Wills, M. I. Katsnelson, I. A. Abrikosov, O. Eriksson, and B. Johansson, Phys. Rev. B **67**, 235105 (2003).

[29] J. M. Wills, O. Eriksson, M. Alouani, and D. L. Price, in *Electronic Structure and Physical Properties of Solids: the Uses of the LMTO method*, edited by H. Dreyssé (Springer-Verlag, Berlin, 2000), vol. 535 of *Lecture Notes in Physics*, pp. 148–67.

[30] A. I. Poteryaev, A. I. Lichtenstein, and G. Kotliar, Phys. Rev. Lett. **93**, 086401 (2004).

[31] J. Minár, L. Chioncel, A. Perlov, H. Ebert, M. I. Katsnelson, and A. I. Lichtenstein, Phys. Rev. B **72**, 045125 (2005).

[32] J. B. Staunton, Psi-k Newsletter **82** (2007).

[33] V. Drchal, V. Janiš, and J. Kudrnovský, Phys. Rev. B **60**, 15664 (1999).

[34] J. F. L. Hopkinson, J. B. Pendry, and D. J. Titterington, Comput. Phys. Commun. **19**, 69 (1980).

[35] J. Braun and M. Donath, J. Phys.: Condens. Matter **16**, S2539 (2004).

[36] V. I. Anisimov, F. Aryasetiawan, and A. I. Lichtenstein, J. Phys.: Condens. Matter **9**, 767 (1997).

[37] M. S. S. Brooks and B. Johansson, J. Phys. F: Met. Phys. **13**, L197 (1983).

[38] T. Miyake and F. Aryasetiawan, Phys. Rev. B **77**, 085122 (pages 9) (2008).

[39] T. Paiva, R. T. Scalettar, C. Huscroft, and A. K. McMahan, Phys. Rev. B **63**, 125116 (2001).

[40] A. Koga, N. Kawakami, T. M. Rice, and M. Sigrist, Phys. Rev. B **72**, 045128 (2005).

[41] M. van Schilfgaarde, T. Kotani, and S. Faleev, Phys. Rev. Lett. **96**, 226402 (pages 4) (2006).